Electronic Supporting Information

Diffusive Confinement of Free Radical Intermediates in the OH Radical Oxidation of Semisolid Aerosol

Aaron A. Wiegel,[a] Matthew J. Liu,[a,b], William D. Hinsberg,[c] Kevin R. Wilson,[†a] and Frances A. Houle[†a]

[a]*Lawrence Berkeley National Laboratory, Chemical Sciences Division, Berkeley, CA, USA 94702*

[b]*University of California, Berkeley, Department of Chemical and Biomolecular Engineering, Berkeley, CA, USA 94702*

[c]*Columbia Hill Technical Consulting, Fremont, CA, USA 94539*

Contents:

S1. Simulation geometry, dynamic volume calculation and role of free volume in diffusion steps
S2. Uncorrected and shape-corrected experimental particle size as a function of OH exposure
S3. Framework validation: simulations of squalane (well mixed liquid) to evaluate effect of compartment size and volume correction method
S4. Calculation of barrier to fragmentation of alkoxy radical with adjacent carboxylic acid group
S5. Semi-detailed description of acyloxy radical fragmentation processes
S6. Determination of evaporation rate coefficients for fragments
S7. Dynamic viscosity measurement of triacontane to estimate self-diffusion coefficient
S8. Maps of peroxy radicals during oxidation
S9. Additional plasticized particle Scenario 2A

S1. Simulation Geometry and Diffusion

A radial core of Cartesian compartments is used to represent the aerosol volume. The volume of each compartment is initialized so that a whole number of molecules will fit in the compartment. In the case of triacontane, using its macroscopic density of 0.81 g cm^{-3} and molecular mass of 422 g mol^{-1}, the molecular volume of triacontane molecule is found to be approximately 8.65×10^{-23} cm^3 $molecule^{-1}$. The number of molecules of triacontane in each compartment is chosen to be 100 molecules, which corresponds to a volume of approximately 8.65×10^{-20} cm^3. Each compartment is set to be a fixed height along the radial axis of the core, 0.5 nm (5×10^{-8} cm). The two orthogonal dimensions are each 1.32×10^{-6} cm. Using this geometry, the average 109 nm diameter triacontane aerosol is simulated using a radial core of 109 0.5 nm thick Cartesian compartments.

We note that for this class of simulation codes, which are a type of kinetic Monte Carlo, the size of the compartment is chosen to provide sufficient spatial resolution while keeping the

calculation to a reasonable size. The core consideration is that a single compartment is treated as well mixed at all times. Thus, the only geometry constraint is that the size of the compartment is small relative to the scale of relevant inhomogenieties in the system. The relative rates of various processes such as a chemical step or gradient-driven transfer of a species between two compartments are unimportant since individual events are randomly selected and propagated one at a time and the time step for each cycle is calculated from the instantaneous reaction rates.[1-3] This consideration is different than that pertinent to finite difference and similar coupled differential equation integration treatments of reaction-diffusion kinetics. In such calculations, a time step is specified and the entire system is evolved at once. Because of the integration process, there are limits to the range of relative rates that can be accurately accommodated in each cycle, and compartment sizes have to be chosen accordingly.

The volume of the particle and thus the compartment volumes change as the reaction proceeds. The instantaneous volume is calculated using the partial volumes of the reactive functional groups defined in the semi-detailed description, the carbon backbone, and free volume components. First, the van der Waals volumes of the two methyl groups and twenty-eight methylene groups from X-ray diffraction data[4] are summed to obtain a value for the van der Waals volume of the triacontane molecule of 5.21×10^{-22} cm^3 $molecule^{-1}$. This value is subtracted from the molecular volume calculated above from the macroscopic density to obtain the free volume of triacontane.[5] This free volume is then divided equally among the thirty carbon atoms to obtain a free volume per carbon of approximately 1.15×10^{-23} cm^3. This value is consistent with previous estimates of the free volume per carbon atom of linear hydrocarbons at room temperature.[6] A separate species termed "bulk" is assigned this free volume per carbon atom and is also used in diffusion as described below. In order to obtain the volume of the functional groups and carbon backbone of triacontane, first, the covalent radius of the hydrogen-carbon bond (110 pm)[7] is used to calculate the volume of a methyl or a methylene hydrogen atom (5.56×10^{-24} cm^3). The volume of two and three hydrogen atoms is then used as the volume of the methylene and methyl groups, respectively. Then, the volume of sixty-two hydrogen atoms is then subtracted from the overall van der Waals volume to obtain the volume of the 30-carbon backbone (1.76×10^{-22} cm^3). In addition, each of the smaller carbon backbones from fragmentation reactions are given a proportional amount of volume of a 30-carbon backbone, e.g. a 23-carbon backbone has a volume that is $23/30^{th}$ of the 30-carbon backbone. Finally, the van der Waals volume from X-ray diffraction[4] of the various functional groups formed after oxidation (carbonyls, alcohols, and carboxylic acids) is used after removing the contribution from a single carbon atom. Notably, defining the volume (and thus density) of the various functional groups and carbon backbones using the associated van der Waals volumes yields the same simple parameterization of the mass density used in previous publications [8, 9] where an addition of an oxygen atom increases the density by 0.03 g cm^{-3}.

Each compartment is assumed to be instantaneously mixed. Species move between compartments according to standard Fickian diffusion kinetics, with the diffusion distance per event calculated from the centers of the two compartments involved. In condensed phases, diffusion is mediated by availability of transient free volumes that allow a molecule to move from one location to another. Free volume is uniform throughout the particle. Accordingly, diffusion of a molecular species (oxidant, functional group, carbon backbone) from a compartment to its neighbor is simulated by an exchange process that requires a free volume

species "bulk" to be available in the adjacent compartment and trade places. If no bulk species are present in a compartment no molecular species can diffuse into it.

The simulation code also supports non-Fickian (environment-sensitive) diffusion kinetics. This was implemented as follows to test the possibility of non-Fickian diffusion in Scenarios 1A and 2A (See Section 9 below).. In these these model scenarios, the production of carbon backbone species with a carbon number less than 16 results in the conversion of the free volume species "bulk" into a separate free volume species "bulk2" that can undergo exchange diffusion with all functional groups and carbon backbones with a different diffusion coefficient of 8.3×10^{-14} cm^2 $molecules^{-1}$ s^{-1}. The species "bulk2" otherwise is treated in the model exactly like the original "bulk" free volume species.

Table S1. Species type and molecular volume of the functional group, carbon number, and free volume species.

Species	Species Type	Molecular volume (cm^3 $molecule^{-1}$)
bulk	Free Volume	1.15×10^{-23}
bulk2[a]	Free Volume	1.15×10^{-23}
site	Free Volume	1.15×10^{-23}
Carbon Atom[b]	Carbon Backbone	5.86×10^{-24}
Aldehyde or Ketone	Functional Group	1.36×10^{-23}
Alcohol	Functional Group	7.50×10^{-24}
Carboxylic Acid	Functional Group	2.66×10^{-23}

[a] Used to describe non-Fickian diffusion. See below for more details

[b] Multiply by the number of carbon atoms to get the total molecular volume for a carbon backbone.

The results from the simulations are corrected to account for the fact that a radial core of constant cross section does not correctly represent the cone appropriate to a spherical particle. The core overweights the contributions to the composition from the compartments toward the center of the particle, and the extent of overweighting decreases as the particle loses mass. The correction is as follows. The thickness of each Cartesian compartment in the radial direction is considered to be the same as the thickness of an equivalent spherical shell. The initial radial (r_i) and final radial coordinates (r_f) are then used to find the volume a spherical shell (V_{shell}) as follows:

$$V_{\text{shell}} = \frac{4}{3}\pi\left(r_f^3 - r_i^3\right). \quad \text{(S1)}$$

The ratio of the volume of the shell and the volume of the Cartesian compartment (V_{box}) is then used to weight the amount of any given species (N) by its position in along the radial axis as follows:

$$N_{\text{corr}} = \frac{V_{\text{shell}}}{V_{\text{box}}} N. \quad \text{(S2)}$$

S2. Uncorrected and shape-corrected experimental particle size as a function of OH exposure

The simulations assume a spherical aerosol particle shape; however, the semisolid triacontane aerosol formed in the experiment is likely non-spherical.[10] In addition, the effective density of the particles derived from the ratio of the vacuum aerodynamic diameter and the mobility diameter of the aerosol is 0.73 g cm^{-3} when the actual density of triacontane is much higher (0.81 g cm^{-3}). Further evidence for a shape change in the aerosol is observed by the sharp discontinuity in the mass in between an OH exposure of 3×10^{11} molecules cm^{-3} s and 10^{12} molecules cm^{-3} s.

To correct for the non-spherical shape of the aerosol for these first few points, a dynamic shape factor was applied to the experimental mass estimate for the unreacted triacontane and the first two points in the oxidation.[11] The dynamic shape factor used for triacontane was 1.07 and based on the ratio of the effective and actual density of the starting material. The first two measured points in the oxidation were assumed to have dynamic shape factors of 1.03 and 1.015, although these are far more uncertain because the actual density of the particles once they are oxidized is unknown. Fortunately, despite this uncertainty, correcting these points for a non-spherical shape is far less important for an accurate model-measurement comparison than correcting the initial triacontane aerosol mass for shape since the data are normalized to the initial mass. After the second measured point in the oxidation, the aerosol is assumed to be spherical with a dynamic shape factor of 1.0. After the initial mass is corrected for shape, the change in aerosol mass upon oxidation becomes much more continuous during the initial stages in oxidation. The corrected and uncorrected mass data, the effective density, and the average volume are given in the Table S4.

Table S2. Experimental data for the oxidation of triacontane aerosol by OH radicals.

OH exposure (molecules cm^{-3} s)	Mobility diameter (nm)	Effective density (g cm^{-3})	Normalized Mass[a]	Dynamic Shape Factor
0	113.2	0.73	1 (1)	1.073
3.07×10^{11}	112.9	0.77	1.02 (1.05)	1.030
6.33×10^{11}	102.7	0.84	1.01 (0.87)	1.015
9.89×10^{11}	97.4	1.04	1.01 (0.91)	1
1.45×10^{12}	95.8	1.13	1.04 (0.94)	1
1.75×10^{12}	95.1	1.17	1.06 (0.95)	1
2.72×10^{12}	91.4	1.30	1.05 (0.94)	1
3.86×10^{12}	87.7	1.41	1.00 (0.90)	1
4.61×10^{12}	86.4	1.47	1.00 (0.90)	1
5.27×10^{12}	87.2	1.49	1.04 (0.93)	1
5.80×10^{12}	83.3	1.51	0.92 (0.82)	1
6.80×10^{12}	82.1	1.53	0.89 (0.80)	1
8.26×10^{12}	81.3	1.53	0.86 (0.78)	1
9.30×10^{12}	80.1	1.55	0.84 (0.75)	1

[a] The uncorrected mass data is shown in parentheses.

S3. Framework validation: simulations of squalane (well mixed liquid) to evaluate effect of compartment size and volume correction method

The validity of the description of uptake and evaporation and the geometry correction for triacontane is tested by predicting full reaction-diffusion kinetics for squalane and comparing it to previously validated results assuming instantaneous mixing.[8]

In our previous work on squalane oxidation, we used two different descriptions. In the first, reaction-diffusion out to 3 generations was simulated using compartments with surface areas of 80 x 80 nm, 1 nm thick and involved explicit adsorption.[12] This study showed that multi-compartment and single-compartment reaction simulations are equivalent for squalane out to 3 generations of oxidation, where volume loss is minimal. In the second, semidetailed simulations of squalane functionalization and fragmentation to 10 generations involved a single compartment and implicit adsorption because the system was well-mixed.[8] We used the semi-detailed mechanism for squalane in a reaction-diffusion model with sixteen 5 nm × 5 nm × 5 nm compartments (equivalent to the 160 nm diameter particle). These compartments are large to make the simulations practical, smaller compartments are computationally much more expensive because of the rapid diffusion kinetics. The choice of larger compartments leads to noticeable discretization (steps) in the simulation results but does not affect their accuracy because the system is well-mixed throughout the reaction, i.e. there are no spatial inhomogeneities in composition.

To perform the test described in this section, one change was made. A pseudo-first order adsorption rate constant of 1.17 s^{-1} is used instead of 10 s^{-1} as in the earlier study.[12] The lower value is due to 2 differences – the compartment area is 0.00391 of that used previously, while the difference in adsorption site definition necessitated by the semi-detailed description increases the rate constant by a factor of 30.

The results in Fig S1 show the agreement is satisfactory, demonstrating that the uptake-evaporation-diffusion kinetics framework used for triacontane, where transport is very slow, is predictive for 10 generations of squalane oxidation where transport is fast.

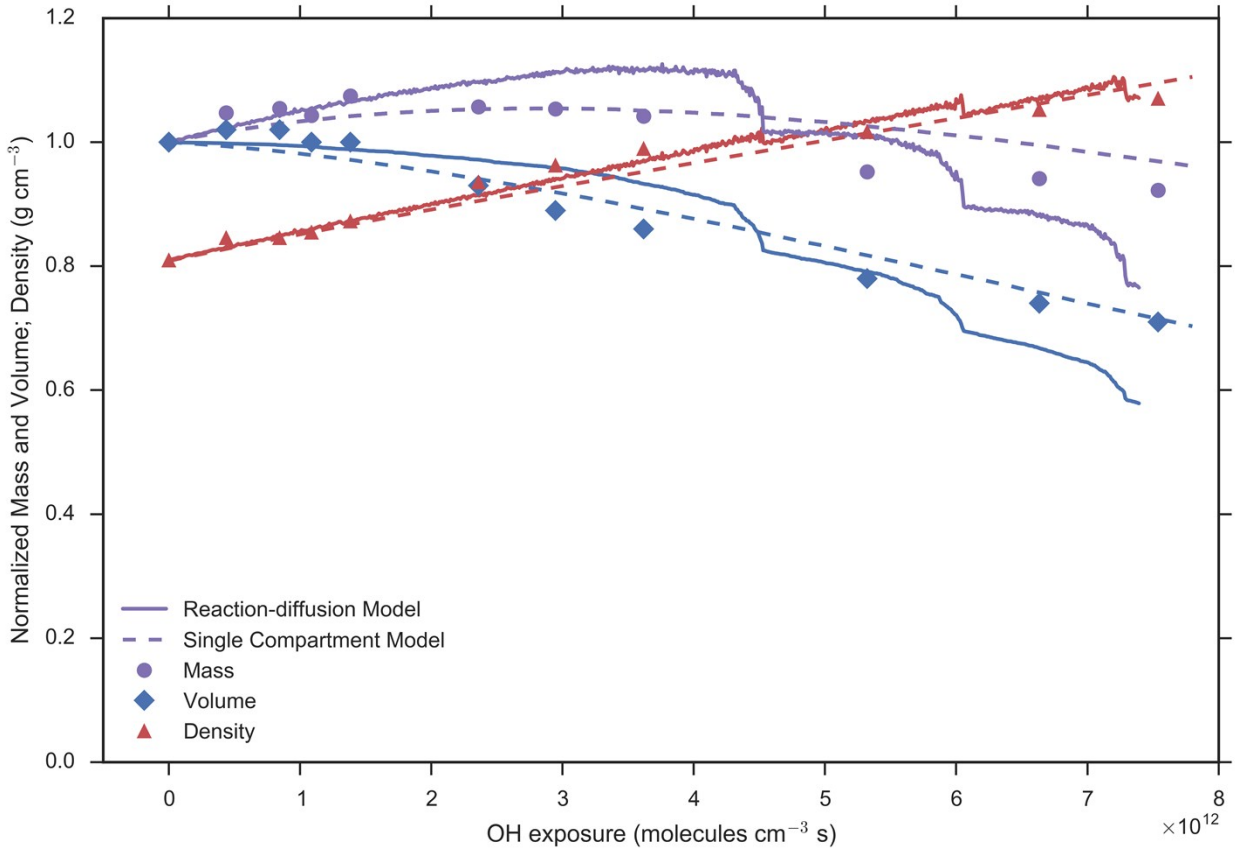

Fig. S1. Comparison of the measured mass, volume, and density of squalane aerosol with the single compartment model from a previous publication[6] and the current reaction-diffusion scheme. Discretization errors from the relatively large compartment size needed to run the simulation in a reasonable time cause the deviations from the single compartment model.

S4. Calculation of barrier to fragmentation of alkoxy radical with adjacent carboxylic acid group

The transition state for the following reaction was calculated to estimate its rate coefficient, which has not been measured:

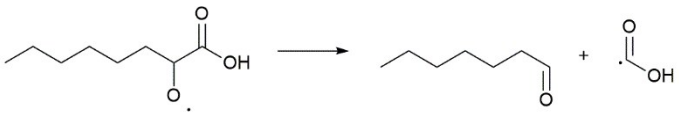

The results of the calculations are presented here.

Alkoxy Radical Ground State

Solvent model: SCF n-Hexadecane

[UB3LYP 6-31G(d,p);FOpt]
HF = -539.5317937

S2 = 0.753384

[UB3LYP 6-31G(d,p);Freq]
HF = -539.5317937
S2 = 0.753384

[Thermochemistry]
Zero-point Correction = 0.223557
Enthalpy Correction = 0.237724
Free Energy Correction = 0.180568

[Geometry]
H 2.050627 0.657783 1.323780
C 0.831978 -0.396493 -0.126754
H 0.898700 -1.361842 0.383780
H 0.863246 -0.608565 -1.202630
C -0.469244 0.325065 0.233593
H -0.468959 1.315737 -0.236432
H -0.500043 0.499197 1.319112
C -1.722068 -0.450758 -0.190486
H -1.691452 -0.622343 -1.275708
H -1.709519 -1.446735 0.274334
C -3.030036 0.262423 0.172854
H -3.041872 1.257998 -0.293051
H -3.060210 0.435845 1.258183
C -4.286529 -0.508724 -0.249794
H -4.273595 -1.503728 0.215515
H -4.256769 -0.681175 -1.334248
C -5.588517 0.209702 0.117143
H -5.645581 1.194309 -0.360731
H -6.465726 -0.364332 -0.198736
H -5.664316 0.364098 1.199590
O 2.143034 1.662670 -0.349386

[Frequencies]

16.5569 37.3625 51.4442
65.1569 98.3920 129.1573
158.6753 161.7396 214.4714
250.8992 277.2465 314.7886
397.8945 424.4328 435.8896
508.3189 584.9527 641.2195
718.8889 736.0859 750.9819
799.3666 842.7848 890.4769
901.8980 955.4984 998.6025
1014.5292 1028.3029 1044.0360

1062.2733 1071.1387 1098.5232
1127.1198 1149.1649 1187.1580
1216.9433 1243.9491 1255.2851
1290.4653 1311.6749 1326.2162
1338.0151 1342.6228 1363.3650
1374.4738 1406.5706 1416.7407
1424.5833 1491.3618 1494.9933
1497.1263 1507.3364 1510.4624
1518.2752 1525.2968 1827.4926
2848.2123 3010.5486 3012.3854
3018.2493 3025.2471 3035.7702
3036.4533 3048.6279 3053.7164
3065.1461 3078.1714 3104.3147
3109.4163 3111.7559 3743.7030

Alkoxy Radical Transition State

Solvent model: SCF n-Hexadecane

[UB3LYP 6-31G(d,p);FTS]
HF = -539.5087462
S2 = 0.765959

[UB3LYP 6-31G(d,p);Freq]
HF = -539.5087462
S2 = 0.765959

[Thermochemistry]
Zero-point Correction = 0.220983
Enthalpy Correction = 0.235700
Free Energy Correction = 0.177186

[Geometry]
C -3.587191 0.574412 0.082177
O -4.678277 -0.160111 -0.005351
H -5.456316 0.428552 -0.084090
O -3.441041 1.758484 0.078320
C -1.916441 -0.774360 0.288277
H -2.112072 -0.728933 1.384752
C -0.779839 0.115012 -0.185785
H -0.874636 1.110845 0.260126
H -0.845603 0.218275 -1.274274
C 0.573759 -0.510362 0.204744
H 0.649249 -1.505366 -0.251407
H 0.604462 -0.665002 1.292461
C 1.771015 0.348806 -0.219683

H 1.740737 0.498706 -1.307884
H 1.676946 1.348333 0.227789
C 3.123114 -0.258729 0.173224
H 3.214776 -1.260321 -0.270461
H 3.152475 -0.406167 1.262337
C 4.323938 0.594712 -0.253248
H 4.229008 1.597098 0.186136
H 4.296942 0.737581 -1.342025
C 5.670935 -0.013312 0.148728
H 5.810055 -1.002190 -0.302966
H 6.506571 0.618120 -0.170339
H 5.742197 -0.134988 1.235642
O -2.306999 -1.762323 -0.357519

[Frequencies]
-268.3432 21.8233 31.0676
54.2662 62.9633 85.3929
122.5265 139.6496 152.7165
186.2395 203.4727 248.8712
251.8820 297.5965 372.2678
445.0261 464.4042 526.6486
581.5477 624.8419 736.3907
751.7426 805.3958 882.3880
898.0351 910.5337 964.1026
1011.3444 1015.6418 1039.2058
1056.2824 1069.1891 1119.5716
1133.6287 1162.4178 1226.7193
1247.0237 1280.5064 1305.0606
1316.0478 1322.2653 1335.3583
1341.0583 1359.8920 1381.3328
1397.9007 1412.9532 1424.7316
1485.7471 1495.2317 1497.3182
1506.7705 1509.7558 1517.3660
1525.2554 1594.4009 1879.1304
2855.0291 3010.9738 3014.9315
3022.2557 3026.3364 3035.8913
3036.1877 3048.3765 3056.6631
3063.4647 3076.0758 3103.6548
3109.2975 3112.9302 3637.5733

S5. Semi-detailed description of acyloxy radical fragmentation processes

When a fragmentation reaction is initially selected by the simulation algorithm, the reaction is separated into three separate steps as shown schematically for R(O)O radicals in Fig. S2. Following loss of CO_2, a neighbouring functional group is randomly selected with a probability proportional to the relative abundance of each group to form the appropriate radical fragment.

For example, if the neighbouring functional group is a ketone, an acyl radical will be formed. Finally, the simulation randomly selects a carbon backbone species with a probability proportional to the relative abundance of each type and a fragmentation step to form smaller carbon fragments. For example, for a secondary RO radical, a 20 carbon backbone may fragment to form two of any of the following possible carbon backbone species: C_2 and C_{18}, C_3 and C_{17}, C_4 and C_{16}, C_5 and C_{15}, C_6 and C_{14}, C_7 and C_{13}, C_8 and C_{12}, C_9 and C_{11}, or two C_{10} species.

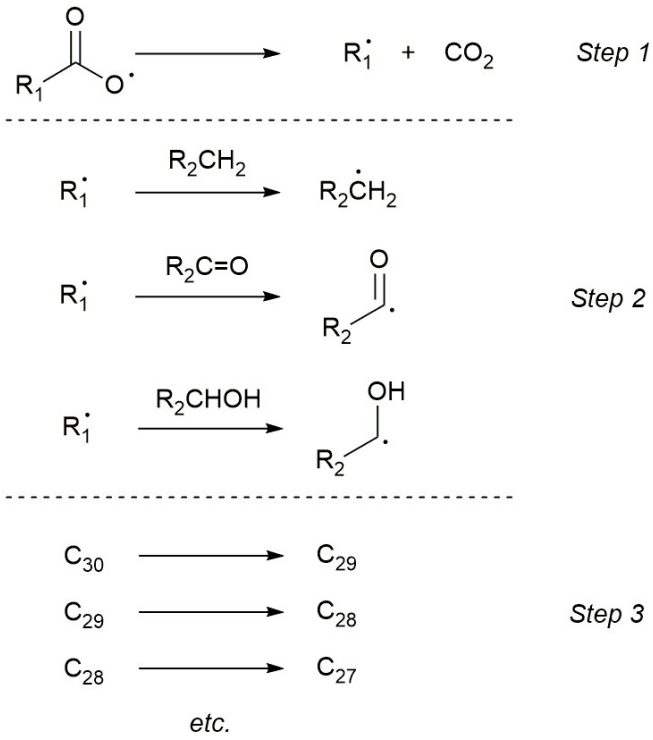

Fig. S2. Schematic representation of acyloxy fragmentation as an example of how the many possibilities of fragmentation are handled in the reaction scheme. First, the alkoxy radical fragments to form CO_2 and a pseudo-intermediate R_1. Then, R_1 "reacts" with an adjacent functional group based on their relative abundance. Finally, a carbon backbone is converted into two separate carbon backbones with a probability based on the relative abundance of the initial backbone.

S6. Determination of evaporation rate coefficients for fragments

Each carbon backbone species has several variants depending on the number of primary functional groups. For example, a 28 carbon backbone has the following variants: C_{28} (one primary functional group), $C_{28}O_2$ (two primary functional groups), $C_{28}COOH$ (one carboxylic

acid group), C_{28}O-COOH (one carboxylic acid group and one primary functional group), and $C_{28}(COOH)_2$ (a dicarboxylic acid).

The evaporation rate coefficients for the fragments are determined from the Hertz-Knudsen equation, Raoult's Law, and the vapor pressure estimated with the EVAPORATION model[10] (p_{sat}) in a similar manner to a previous publication.[6] Here, the simulated volume (V_{sim}) and area (A_{sim}) are used with the flux to obtain the following equation for the evaporation rate coefficient (k_{evap}):

$$k_{evap} = \frac{\alpha p_{sat} A_{sim}}{V_{sim}[RH]} \sqrt{\frac{N_A}{2\pi M k_B T}}, \quad \text{(S3)}$$

where α is the accommodation coefficient (assumed to be 1), [RH] is the initial molecular density of triacontane, N_A is avogadro's number, M is the molecular mass of the evaporating species. Since primary alcohols and aldehydes have evaporation rate coefficients within an order of magnitude of each other, they are lumped together as a single carbon backbone species for the purposes of evaporation. The coefficients are presented in Table S3.

Table S3. Rate coefficients for evaporation of species based on their carbon number and primary functional groups.

Carbon number	k_{1prim} (s^{-1})	k_{2prim} (s^{-1})	k_{COOH} (s^{-1})	$k_{1prim,COOH}$ (s^{-1})	k_{diacid} (s^{-1})
2	2.6×10^{6}	1.4×10^{5}	1.1×10^{5}	6.1×10^{3}	3.9
3	7.5×10^{5}	4.2×10^{4}	3.1×10^{4}	1.8×10^{3}	6.4×10^{-2}
4	2.2×10^{5}	1.3×10^{4}	9.4×10^{3}	5.5×10^{2}	6.6×10^{-3}
5	6.6×10^{4}	3.9×10^{3}	2.9×10^{3}	1.7×10^{2}	1.1×10^{-1}
6	2.0×10^{4}	1.2×10^{3}	8.8×10^{2}	5.3×10^{1}	1.5×10^{-3}
7	6.2×10^{3}	3.7×10^{2}	2.7×10^{2}	1.6×10^{1}	7.4×10^{-3}
8	1.9×10^{3}	1.1×10^{2}	8.5×10^{1}	5.1	1.7×10^{-4}
9	5.9×10^{2}	3.6×10^{1}	2.7×10^{1}	1.6	8.0×10^{-4}
10	1.9×10^{2}	1.1×10^{1}	8.3	5.0×10^{-1}	7.7×10^{-6}
11	5.8×10^{1}	3.5	2.6	1.6×10^{-1}	2.4×10^{-6}
12	1.8×10^{1}	1.1	8.3×10^{-1}	5.0×10^{-2}	7.7×10^{-7}
13	5.7	3.5×10^{-1}	2.6×10^{-1}	1.6×10^{-2}	2.4×10^{-7}
14	1.9	1.1×10^{-1}	8.3×10^{-2}	5.1×10^{-3}	7.8×10^{-8}
15	5.8×10^{-1}	3.6×10^{-2}	2.6×10^{-2}	1.6×10^{-3}	2.5×10^{-8}
16	1.8×10^{-1}	1.1×10^{-2}	8.4×10^{-3}	5.1×10^{-4}	7.9×10^{-9}
17	5.9×10^{-2}	3.6×10^{-3}	2.7×10^{-3}	1.6×10^{-4}	-
18	1.9×10^{-2}	1.2×10^{-3}	8.5×10^{-4}	5.3×10^{-5}	-
19	6.0×10^{-3}	3.7×10^{-4}	2.7×10^{-4}	1.7×10^{-5}	-
20	1.9×10^{-3}	1.2×10^{-4}	8.7×10^{-5}	5.4×10^{-6}	-
21	6.1×10^{-4}	3.8×10^{-5}	2.8×10^{-5}	1.7×10^{-6}	-
22	2.0×10^{-4}	1.2×10^{-5}	8.9×10^{-6}	5.5×10^{-7}	-
23	6.3×10^{-5}	3.9×10^{-6}	2.9×10^{-6}	1.8×10^{-7}	-
24	2.0×10^{-5}	1.2×10^{-6}	9.2×10^{-7}	5.7×10^{-8}	-

25	6.4×10^{-6}	4.0×10^{-7}	3.0×10^{-7}	1.8×10^{-8}	-
26	2.1×10^{-6}	1.3×10^{-7}	9.5×10^{-8}	5.9×10^{-9}	-
27	6.7×10^{-7}	4.1×10^{-8}	3.1×10^{-8}	1.9×10^{-9}	-
28	2.1×10^{-7}	1.3×10^{-8}	9.9×10^{-9}	6.1×10^{-10}	-
29	6.9×10^{-8}	4.3×10^{-9}	3.2×10^{-9}	2.0×10^{-10}	-
30	2.2×10^{-8}	1.4×10^{-9}	1.0×10^{-9}	6.4×10^{-11}	-

As evaporation proceeds, compartments are emptied of molecules and the active surface of the aerosol particle retreats toward the center of the particle. To simulate this process, evaporation is only allowed when (adsorption) sites are present in the compartment. These are defined at the start of the simulation in the top compartment only, and are created in lower compartments. As the carbon backbone and associated functional groups are converted into gas phase species by evaporation, a number of "bulk" free volume species equal to the number of carbons is converted into surface sites. If there are no remaining "bulk" species in the same compartment, then ones in the next compartment are converted to surface sites. In the process, an additional species termed "gas" is formed that helps define the location of the interface. Because of the statistical nature of event selection, occasionally a species associated with the condensed phase (i.e. a functional group or carbon backbone) can be found in a compartment above the one containing a "gas" species. When this occurs the gas and condensed phase species immediately exchange places to prevent residual condensed phase material remaining in compartments that have become disconnected from the particle.

S7. Dynamic viscosity measurement of triacontane to estimate self-diffusion coefficient

The dynamic viscosity of pure, solid triacontane (98% purity, Sigma-Aldrich) was measured as a function of plate oscillation using a Parallel Plate TA Instruments Discovery Hybrid Series DHR-2 Rheometer with an 8 mm plate geometry. An 8 mm ID O-ring was placed atop the Peltier plate of the rheometer, directly below the plate geometry. The temperature of the Peltier plate was maintained at 72°C, which is 5°C greater than the upper end of the melting point range of triacontane (67°C). The triacontane sample was first melted separately in a beaker on a hot plate at 90°C and then poured into the O-ring. The plate geometry was lowered slowly until touched with the liquid sample at the trim gap of 1550 μm. The Peltier plate was then cooled to 25°C. To ensure firm contact with the cooled, compacted solid sample, the plate geometry was lowered 50 μm to the measurement gap of 1500 μm. At this height, the plate geometry was unable to freely rotate if turned. A logarithmic sweep from 10 to 10^{-3} rad s^{-1} using a displacement of approximately 10^{-3} radians was used to find the loss modulus (G'') and thus dynamic viscosity (η') of triacontane as a function of oscillation frequency (ω). The results from these measurements were then used estimate the zero-shear limit of the dynamic viscosity (η_0) and the self-diffusion coefficient of triacontane as follows:[13]

$$\eta_0 = \lim_{\omega \to 0} \frac{G''}{\omega} \qquad \text{(S4)}$$

The results of one set of these measurements is shown in Fig. S3.

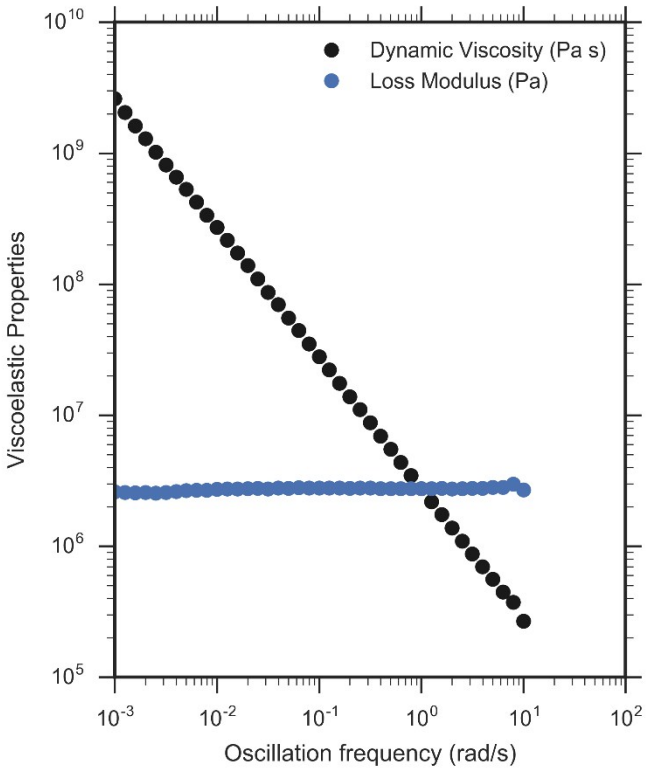

Fig. S3. The loss modulus and dynamic viscosity of triacontane as a function of the oscillation frequency.

S8. Maps of peroxy radicals during oxidation

The calculated spatial distributions of peroxy radicals formed during triacontane oxidation using Scenarios 1 and 1A are plotted in Figures S4 and S5, respectively. It is clear that active reactions are strictly confined to the surface in Scenario 1 while they can occur throughout the particle in Scenario 1A.

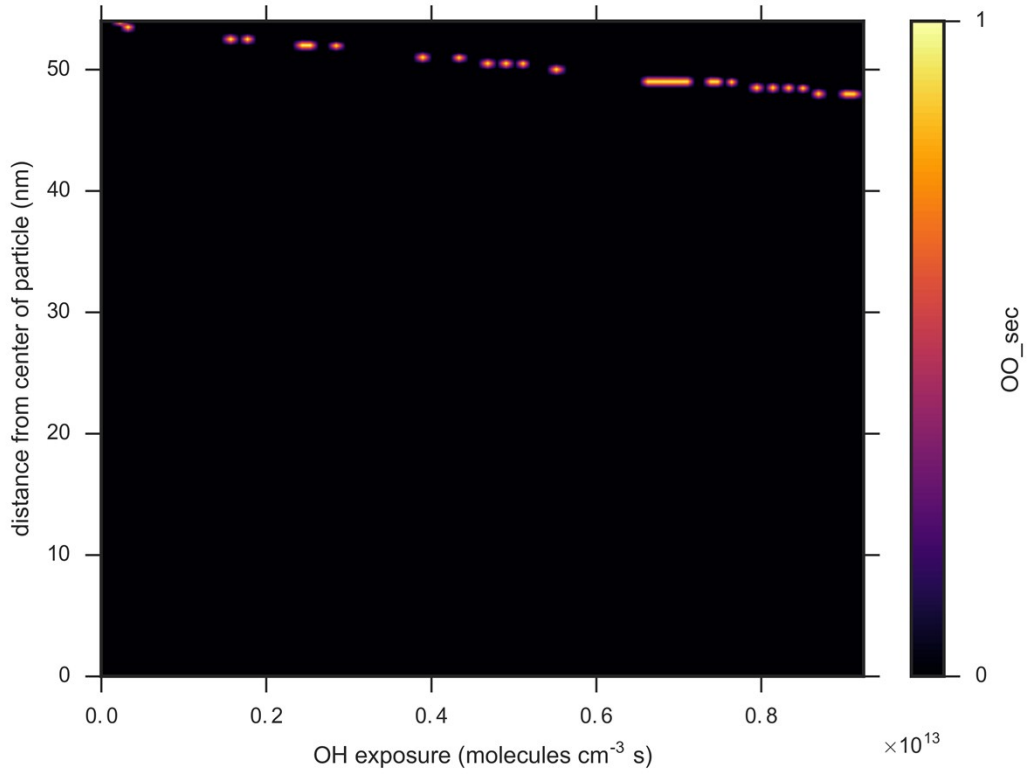

419

420 **Figure S4**. Plot of peroxy radical concentrations as a function of position and OH exposure under
421 Scenario 1. The radicals are confined to the surface of the reacting aerosol particle.

422

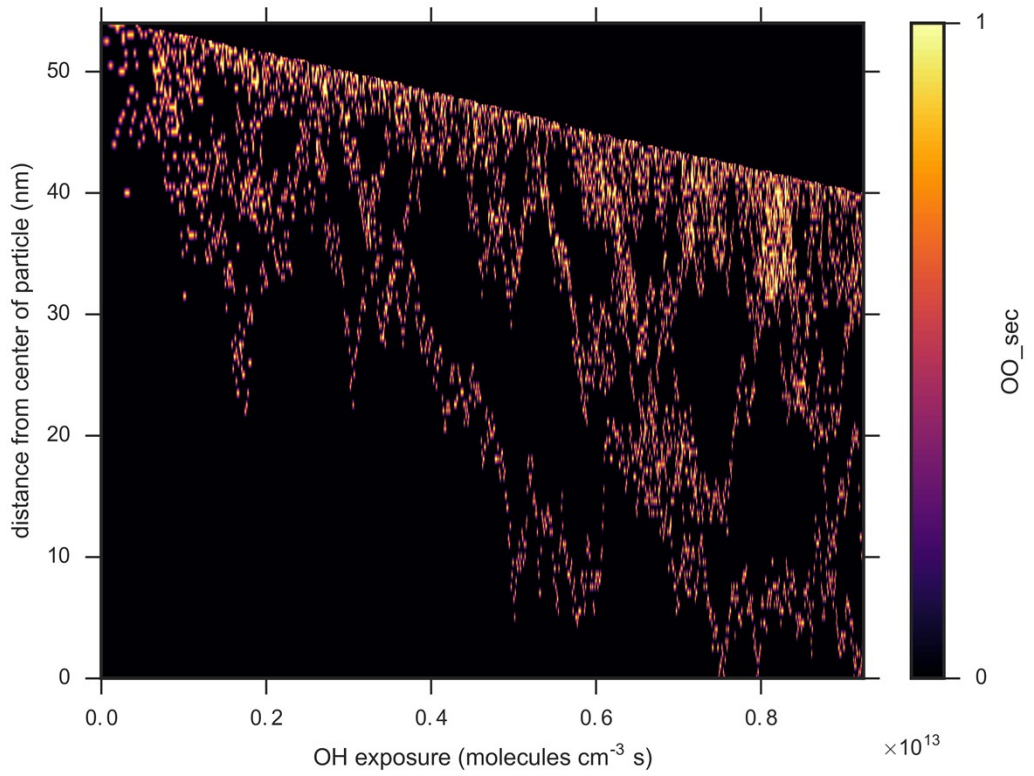

Figure S5. Plot of peroxy radical concentrations as a function of position and OH exposure under Scenario 1A. The radicals are found throughout the reacting particle.

S9. Additional plasticized particle Scenario 2A

Scenario 2A is analogous to Scenario 1A and evaluates the effect of plasticization during exposure to OH when the gas-phase value for the OH + CO(OH) reaction rate coefficient is used. Simulation results are shown in Figures S6 and S7. When the particle is 145nm in diameter, the agreement between triacontane disappearance for Scenarios 1A and 2A is comparable. When it is 109nm in diameter however, the differences are dramatic. The increased value of $k_{OH+COOH}$ in Scenario 2A can improve the agreement between the predicted and measured carbon and hydrogen content, but the agreement with the mass and oxygen content is not as good as in Scenario 1A.

Further investigation of Scenarios 1A and 2A reveals why Scenario 1A, which involves plasticization with oxidation, best predicts the measured effective uptake coefficient, aerosol mass, and elemental composition. As shown in Fig. 10, the internal distribution of oxidized material extends approximately 20 nm into the aerosol with a peak value of 0.6 at the surface at an OH exposure of 2×10^{12} molecules cm^{-3} s while the average O/C ratio is 0.2. The broader internal distribution of oxidation limits the fragmentation chemistry and subsequent evaporation of volatile material from the particle. An unreacted core of the starting material remains in the inner 30 nm of the aerosol. Increasing the relative importance of fragmentation reactions as in Scenario 2A promotes more volatilization of otherwise non-volatile carboxylic acids and leads to

a too-rapid disappearance of triacontane and low extent of oxidation relative to experiment. It is clear that the overall transformation kinetics are very sensitive to the balance between surface reactions when the particle is highly oxidized, and internal transport.

Figure S6. Triacontane disappearance curve for a 145 nm particle, predicted under Scenario 2A with an adsorption rate coefficient for OH of 10 s^{-1}. The results are to be compared to Figure 4.

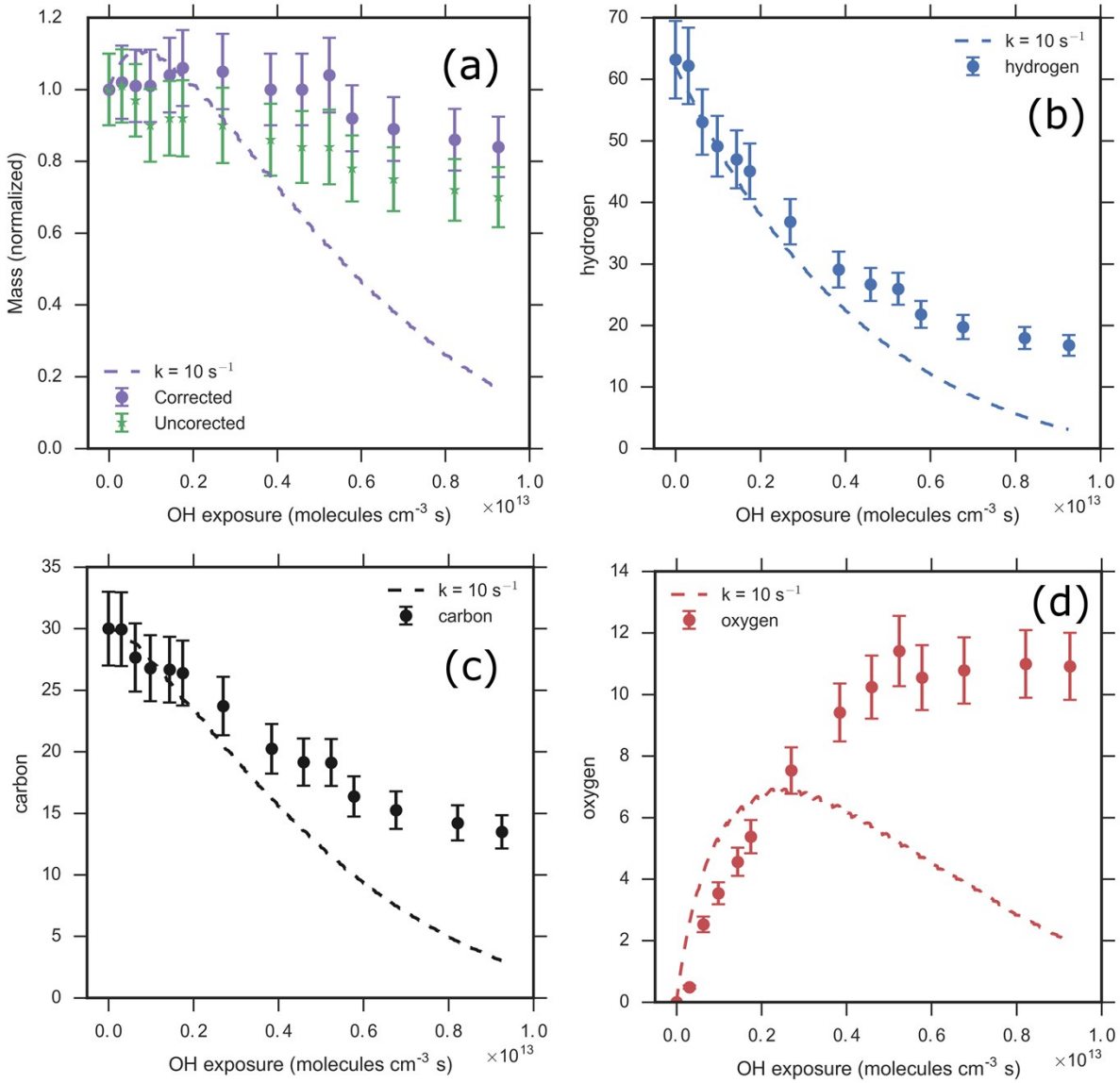

Figure S7. Simulation results for a 109 nm particle, predicted under Scenario 2A with an adsorption rate coefficient for OH of 10 s^{-1}.,(a) Mass, (b) H content per molecule, (c) C content per molecule and (d) O content per molecule. The results are to be compared to Figures 5, 6, and 8.

References

1. D. Bunker, B. Garrett, T. Kleindienst and G. L. III, *Combustion and Flame*, 1974, **23**, 373-379.
2. D. T. Gillespie, *J Comput Phys*, 1976, **22**, 403-434.
3. F. A. Houle, W. D. Hinsberg, M. Morrison, M. I. Sanchez, G. Wallraff, C. Larson and J. Hoffnagle, *Journal of Vacuum Science & Technology B: Microelectronics and Nanometer Structures*, 2000, **18**, 1874.
4. A. Bondi, *The Journal of Physical Chemistry*, 1964, **68**, 441-451.
5. M. H. Cohen and D. Turnbull, *The Journal of Chemical Physics*, 1959, **31**, 1164-1169.
6. A. K. Doolittle, *J Appl Phys*, 1951, **22**, 1471-1475.
7. B. Cordero, V. Gómez, A. E. Platero-Prats, M. Revés, J. Echeverría, E. Cremades, F. Barragán and S. Alvarez, *Dalton Transactions*, 2008, DOI: 10.1039/b801115j, 2832-2838.
8. A. A. Wiegel, K. R. Wilson, W. D. Hinsberg and F. A. Houle, *Phys. Chem. Chem. Phys.*, 2015, **17**, 4398-4411.
9. K. R. Wilson, J. D. Smith, S. H. Kessler and J. H. Kroll, *Phys Chem Chem Phys*, 2012, **14**, 1468-1479.
10. Y. Katrib, G. Biskos, P. R. Buseck, P. Davidovits, J. T. Jayne, M. Mochida, M. E. Wise, D. R. Worsnop and S. T. Martin, *The Journal of Physical Chemistry A*, 2005, **109**, 10910-10919.
11. P. F. DeCarlo, J. G. Slowik, D. R. Worsnop, P. Davidovits and J. L. Jimenez, *Aerosol Science and Technology*, 2004, **38**, 1185-1205.
12. F. A. Houle, W. D. Hinsberg and K. R. Wilson, *Phys. Chem. Chem. Phys.*, 2015, **17**, 4412-4423.
13. C. B. Gell, W. W. Graessley and L. J. Fetters, *Journal of Polymer Science Part B: Polymer Physics*, 1997, **35**, 1933-1942.